Electronic Supplementary Information

for

Solar H_2 Generation *via* ethanol photoreforming on ε-Fe_2O_3 Nanorod Arrays Activated by Ag and Au Nanoparticles

Giorgio Carraro,[a] Alberto Gasparotto,[a] Chiara Maccato,[a] Valentina Gombac,[b] Francesca Rossi,[c] Tiziano Montini,[b] Daniel Peeters,[a,d] Elza Bontempi,[e] Cinzia Sada,[f] Davide Barreca,[g,*] and Paolo Fornasiero[b,h,*]

[a] *Department of Chemistry, Padova University and INSTM, Via Marzolo, 1 - 35131 Padova, Italy.*

[b] *Department of Chemical and Pharmaceutical Sciences, ICCOM-CNR Trieste Research Unit - INSTM Research Unit, University of Trieste, via L. Giorgieri 1, 34127 Trieste, Italy.*

[c] *CNR-IMEM, Parco Area delle Scienze, 43124 Parma, Italy.*

[d] *Inorganic Chemistry II, Department of Chemistry and Biochemistry, Ruhr-University Bochum, 44801 Bochum, Germany.*

[e] *Chemistry for Technologies Laboratory, Brescia University, 25123 Brescia, Italy.*

[f] *Department of Physics and Astronomy, Padova University, Via Marzolo, 1 - 35131 Padova, Italy.*

[g] *CNR-IENI and INSTM, Department of Chemistry, Padova University, Via Marzolo, 1 - 35131 Padova, Italy.*

[h] *King Abdullah University of Science and Technology, Thuwal 23955-6900, Saudi Arabia.*

* Authors to whom correspondence should be addressed; e-mail: davide.barreca@unipd.it; pfornasiero@units.it.

EXPERIMENTAL SECTION

1. Synthesis

A cold-wall horizontal chemical vapor deposition (CVD) apparatus[1] was adopted for the synthesis of iron(III) oxide systems, using $Fe(hfa)_2TMEDA$ as a molecular source (hfa = 1,1,1,5,5,5 - hexafluoro - 2,4 - pentanedionate; TMEDA = *N*,*N*,*N*′,*N*′ – tetramethylethylenediamine; vaporization temperature = 60 °C).[2,3] Basing on preliminary experiments,[4,5] growth temperature and total pressure were set to 400 °C and 10.0 mbar, respectively. Precursor vapors were transported towards the deposition zone by means of an O_2 flow (purity = 6.0; rate = 100 sccm) through connection gas lines, maintained at 120 °C in order to prevent detrimental condensation phenomena. An auxiliary oxygen flow (rate = 100 sccm) was introduced separately into the reaction chamber, after passing through a water reservoir maintained at 50 °C. Under these conditions, the H_2O partial pressure was estimated to be ≈1.5 mbar.[6] Depositions were carried out for a total duration of 60 min on Si(100) substrates (MEMC®, Merano, Italy, 10 mm × 10 mm × 1 mm), subjected to a cleaning procedure before each experiment (including a treatment for 5 minutes in a 2 % HF solution). In spite of the etching procedure, the formation of an SiO_2 layer (thickness ≈ 2 nm) on the surface of Si(100) substrates was unavoidable in the reaction condition. Due to the appreciably higher thickness of the overlying Fe_2O_3 deposits, it is not expected to provide an appreciable contribution, or could even have some beneficial influence on the ultimate system performances.[7] Subsequently, gold and silver deposition on iron oxide samples was performed by a custom-built Radio Frequency (RF) plasmochemical reactor (ν = 13.56 MHz) [8] using Ar (purity = 5.0) as plasma source. Gold (BAL-TEC AG, 99.99 %) or silver (Alfa Aesar, 99 %) targets (thickness = 0.3 mm in both cases) were fixed on the RF electrode, and supported ε-Fe_2O_3 matrices were mounted on a second grounded electrode. Sputtering processes were carried out under the following conditions: substrate temperature = 60 °C; RF-power = 5 W; total pressure = 0.3 mbar; Ar flow rate = 10 sccm. After

optimization of the processing parameters, experiment duration was set at 30 and 45 min for Au and Ag, respectively to achieve a comparable metal loading. Finally, *ex-situ* annealing in air at 400 °C for 1 h was performed in order to thermally stabilize the above nanosystems before functional tests.

2. Material Characterization

Two-dimensional X-ray diffraction (2D-XRD) images were recorded by means of a D-max-RAPID X-ray microdiffractometer equipped with a cylindrical imaging plate detector, enabling to collect diffraction data in the ranges $2\vartheta = 0 - 160°$ (horizontally) and $2\vartheta = -45 - +45°$ (vertically) upon using Cu Kα radiation. The incident beam collimators enable different spot sizes to be projected onto the sample. In this work, measurements were made in reflection mode, adopting a collimator diameter of 300 μm and an exposure time of 30 min for each 2D-XRD image.

Field emission scanning electron microscopy (FE-SEM) micrographs were collected by a Zeiss SUPRA 40VP instrument, using primary beam acceleration voltages of 10 kV. Line-scan energy dispersive X-ray spectroscopy (EDXS) analyses were carried out by monitoring the Fe Kα, O Kα, and Au Lα/Ag Lα signals throughout the deposit thickness by an Oxford INCA x-sight X-ray detector (acceleration voltage = 20.0 kV).

Transmission electron microscopy (TEM) measurements were performed by a JEOL 2200FS field-emission microscope operated at 200 kV. High Angle Annular Dark Field (HAADF) images (also called *Z*-contrast images [9] were acquired in scanning TEM (STEM) mode, setting the convergence semiangle to 11.9 mrad, the inner detection semiangle to 75 mrad, and the probe size to 0.5 nm. All the experiments were carried out on cross-sectional specimens prepared by conventional mechanical grinding and polishing, down to the thickness of approximately 30 μm, followed by Ar ion milling.

X-ray photoelectron spectroscopy (XPS) analyses were performed by a Thermo Scientific K-Alpha KA1066 spectrometer, using a standard Al Kα source (hν =1486.6 eV) powered at 250 W, at a

working pressure lower than 10^{-9} mbar. The reported Binding Energy (BE) values were corrected for charging effects by assigning a BE of 284.8 eV to the adventitious C1s signal. Gold and silver molar fractions were calculated as X_M = [(M at.%) / (M at.% + Fe at.%)×100], with M = Ag, Au. Secondary ion mass spectrometry (SIMS) analyses were carried out by means of a IMS 4f mass spectrometer (Cameca) using a 14.5 keV Cs^+ primary beam (current = 20 nA) and by negative secondary ion detection, using an electron gun for charge compensation. Beam blanking mode and high mass resolution configuration were adopted. Signals were recorded rastering over a 150×150 μm^2 area, detecting secondary ions from a sub-region close to 7×7 μm^2 to avoid crater effects.

3. Photocatalytic activity

The photoreforming activity of the bare and M-loaded ε-Fe_2O_3 (M = Au, Ag) specimens was evaluated under simulated sunlight irradiation using the experimental apparatus previously described.[10] Illumination was performed using a Solar Simulator (LOT-Oriel) equipped with a 150 W Xe lamp, filtered using an Atmospheric Edge filter to reduce the UV photons below 300 nm. In this way, the light intensity for simulated sunlight experiments, measured by a radiometer, was ≈25 and ≈180 mW cm^{-2} in the 250 – 400 nm (UV-A) and in the 400 – 1000 nm ranges, respectively. For experiments under the sole Vis irradiation, a 420 nm cut-off filter was used (AM-79765). The samples were mounted on a sample holder and placed on the botton of the reactor, filled with 80 mL of ethanol/water 1:1 (v/v) solution. All the experiments were performed with the photoreactor immersed in a thermostatic bath at 25 °C. Gaseous products (H_2, CO_2, etc) were removed by an Ar flow (15 mL×min^{-1}) and on-line detected by an Agilent 7890 Gas Chromatographer (GC), equipped with a 10 way-two loop injection valve. H_2 analysis was performed by means of a Carboxen 1010 PLOT column (Supelco, 30 m × 0.53 mm ID, 30 μm film) connected to Thermal Conductivity Detector (TCD), using Ar as carrier gas. Conversely, the analysis of CO_2 and volatile compounds in

the gas flow was performed using a DB522-ms capillary column (J&W, 60 m × 0.32 mm ID, 20 μm film) connected to an Agilent 5975C MS detector, using He as carrier gas.

Analysis of the liquid phase was performed using an Agilent 7890A GC system (column: J&W DB-225 ms, 60 m, 0.25 mm, 0.25 mm) coupled with a 5975C VL MSD with triple-Axis Detector.

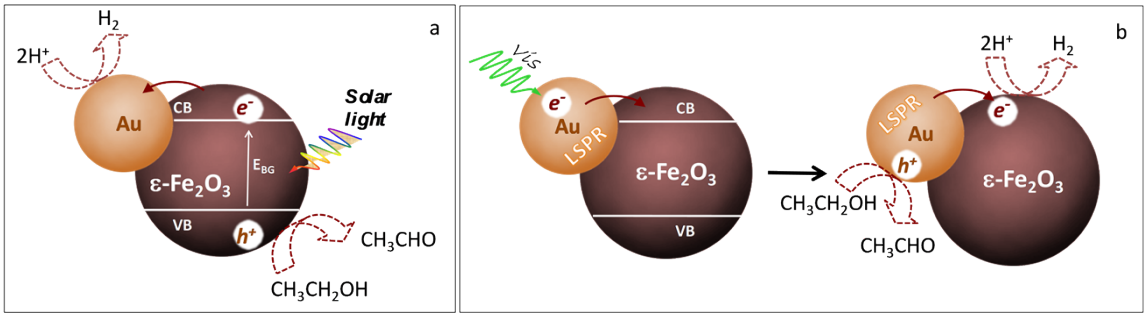

Scheme S1. Sketch of the main processes occurring on Au/ε-Fe_2O_3 under (a) simulated solar illumination and (b) Vis light irradiation. In the latter case, the process is initiated by gold LSPR absorption.

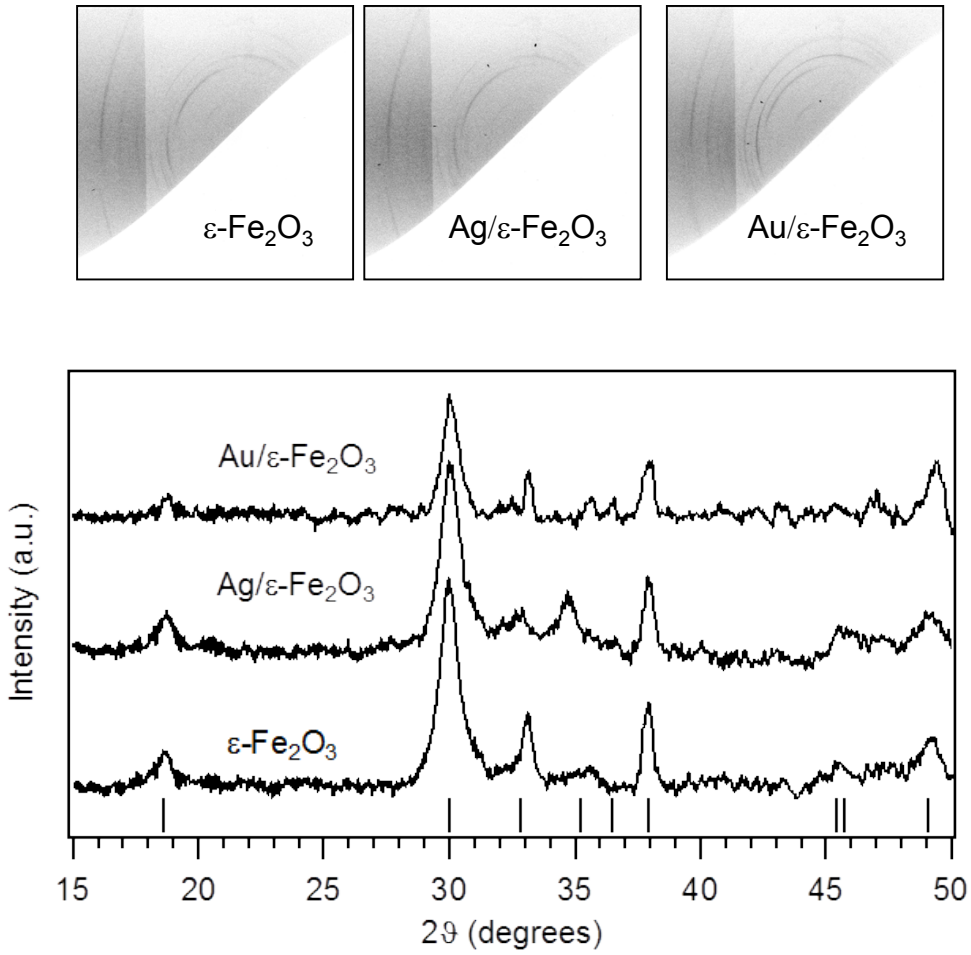

Figure S1. 2D-XRD images and integrated XRD patterns of ε-Fe_2O_3, Ag/ε-Fe_2O_3 and Au/ε-Fe_2O_3. The diffraction patterns displayed the reflections located at 2ϑ = 18.7°, 30.1°, 33.1°, 34.8°, 37.9°, 49.2° (d_{hkl} = 2.40, 1.54, 1.41, 1.35, 1.25, 1.02 Å, respectively), that are assigned respectively to the (002), (013), (122), (113), (211)/(004), (142)/(015) reflections of orthorhombic ε-Fe_2O_3 structure. The reflections expected for this polymorph have been marked by black vertical bars.[11]

ε-Fe_2O_3 (*present work*)			α-Fe_2O_3[12]			γ-Fe_2O_3[13]		
2ϑ (°)	(hkl)[11]	Intensity[11]	*2ϑ (°)*	(hkl)	Intensity	*2ϑ (°)*	(hkl)	Intensity
18.7	(002)	40						
			24.1	(012)	30			
30.1	(013)	85						
						30.2	(220)	35
33.1	(122)	100						
			33.2	(104)	100			
34.8	(113)	41						
			35.6	(110)	70	*35.6*	(311)	100
37.9	(211) / (004)	12 / 70						
			40.9	(113)	20			
						43.3	(400)	16
49.2	(142) / (015)	88 / 50						
			49.5	(024)	40			

Table S1. XRD reflections of the ε-Fe_2O_3 polymorph measured in the present work, compared with the most intense ones reported for α-Fe_2O_3 and γ-Fe_2O_3, in the angular range 15-50°. Miller indexes and relative intensities (only for peaks with relative intensities ≥ 10) are also reported.

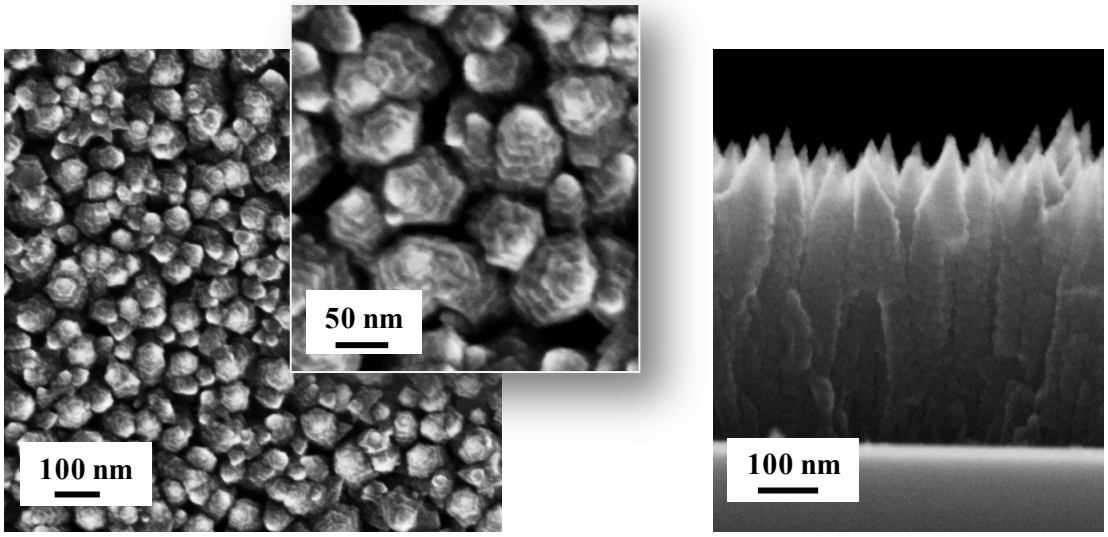

Figure S2. Representative plane-view and cross-sectional FE-SEM micrographs for bare ε-Fe_2O_3 nanorod arrays.

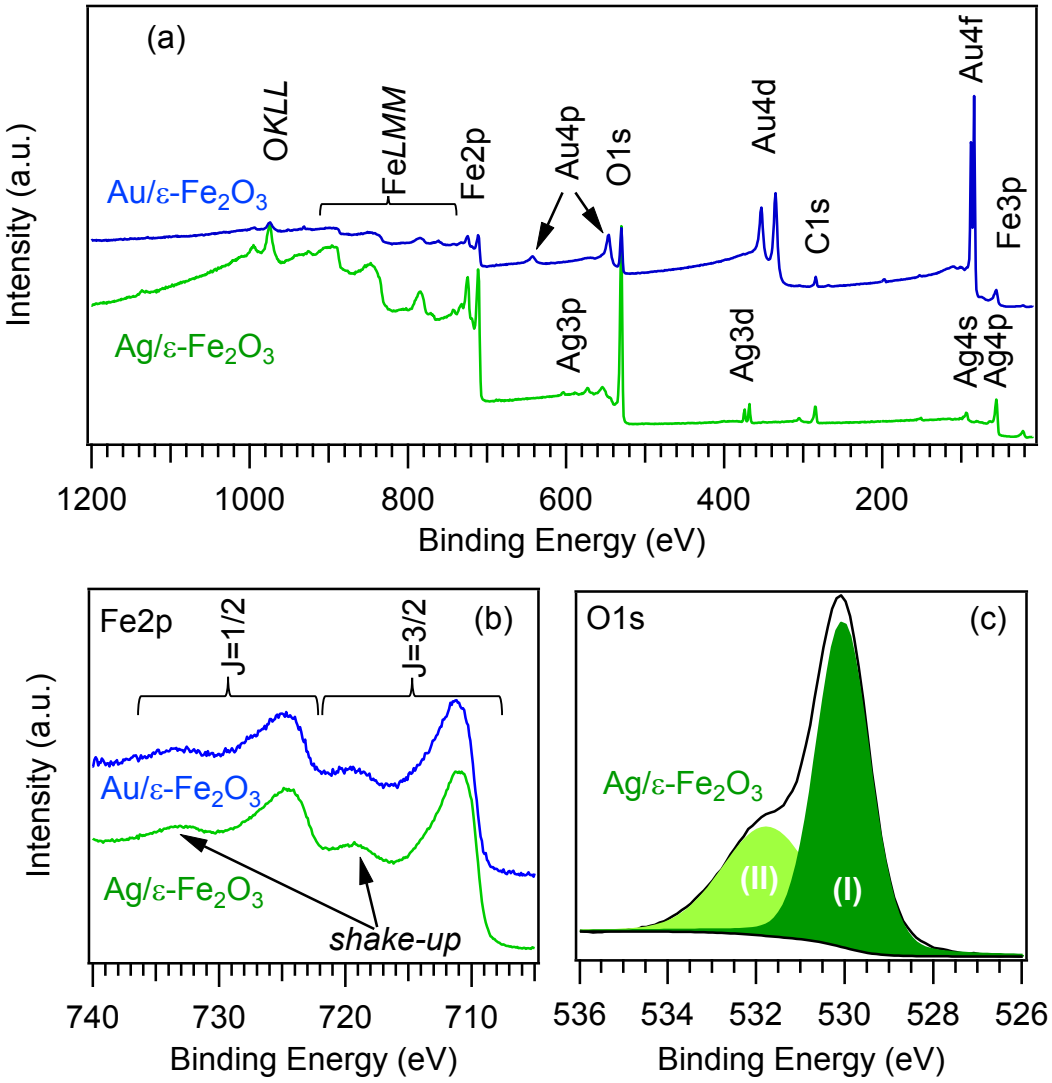

Figure S3. (a) XPS survey and (b) Fe2p surface signals for Ag/ε-Fe_2O_3 and Au/ε-Fe_2O_3 nanosystems. (c) Surface O1s signal for Ag/ε-Fe_2O_3 systems.

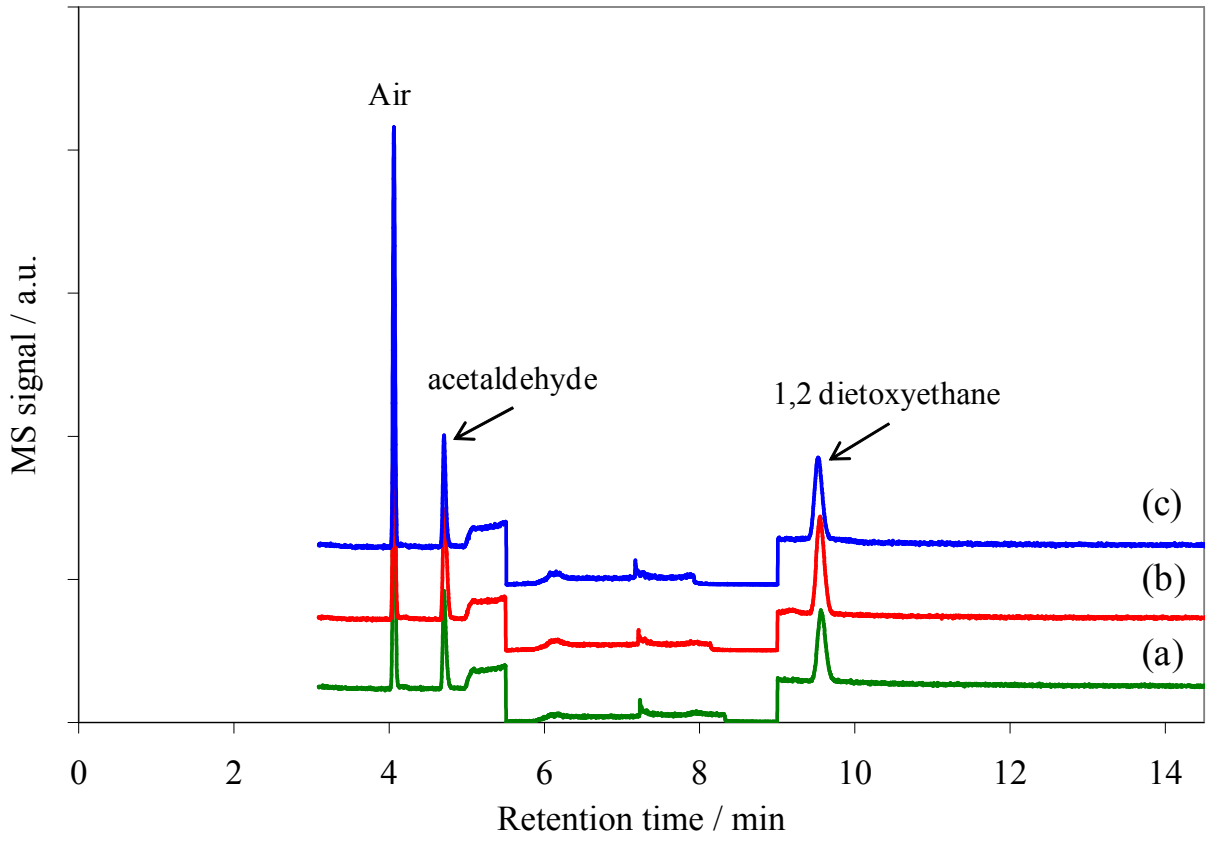

Figure S4. GC/MS analysis of aqueous solutions collected after ethanol photoreforming using (a) ε-Fe_2O_3, (b) Au/ε-Fe_2O_3 and (c) Ag/ε-Fe_2O_3. From 5.5 to 9.0 minutes the ethanol peak is suppressed by the quadrupole filter.

References

1. D. Barreca, A. Gasparotto, C. Maragno, E. Tondello, C. Sada, *Chem. Vapor Depos.*, 2004, **10**, 229.
2. D. Barreca, G. Carraro, A. Devi, E. Fois, A. Gasparotto, R. Seraglia, C. Maccato, C. Sada, G. Tabacchi, E. Tondello, A. Venzo, M. Winter, *Dalton Trans*., 2012, **41**, 149.
3. D. Barreca, G. Carraro, A. Gasparotto, C. Maccato, R. Seraglia, G. Tabacchi, *Inorg. Chim. Acta*, 2012, **380**, 161.
4. G. Carraro, C. Maccato, E. Bontempi, A. Gasparotto, O. I. Lebedev, S. Turner, L. E. Depero, G. Van Tendeloo, D. Barreca, *Eur. J. Inorg. Chem.*, 2013, **2013**, 5454.
5. G. Carraro, D. Barreca, C. Maccato, E. Bontempi, L. E. Depero, C. De Julián Fernández, A. Caneschi, *CrystEngComm*, 2013, **15**, 1039.
6. D. Barreca, A. Gasparotto, C. Maragno, E. Tondello, E. Bontempi, L. E. Depero, C. Sada, *Chem. Vapor Depos.*, 2005, **11**, 426.
7. I. Thomann, B. A. Pinaud, Z. Chen, B. M. Clemens, T. F. Jaramillo, M. L. Brongersma, *Nano Lett.*, 2011, **11**, 3440.
8. D. Barreca, A. Gasparotto, E. Tondello, C. Sada, S. Polizzi, A. Benedetti, *Chem. Vapor Depos.*, 2003, **9**, 199.
9. P. D. Nellist, S. J. Pennycook, *Adv. Imaging Electron Phys.*, 2000, **113**, 147.
10. G. Carraro, C. Maccato, A. Gasparotto, T. Montini, S. Turner, O. I. Lebedev, V. Gombac, G. Adami, G. Van Tendeloo, D. Barreca, P. Fornasiero, *Adv. Funct. Mater.* 2014, **24**, 372.
11. Pattern n°51122, ICSD (2007).
12. Pattern n°33-0664, JCPDS (2000).
13. Pattern n°39-1346, JCPDS (2000).